Supplementary Information

Atomically Precise Alloy AgCu Cuboid Nanocluster with Cubic Core: Gram Scale Synthesis, Total Structure, Electronic Structure, and Catalytic Performance

Abhijit Nag[†, ‡], Abdul Mannan Butt[†, ‡], Moon Young Yang[§], Praveen B. Managutti[‡, #], Bilal Masood Pirzada[‡], M. Infas H. Mohideen [†, ‡], Ahmed L. Abdelhady[†, ‡], Mohamed Abu Haija[†, ‡], Sharmarke Mohamed[†, ‡, #], Boris V. Merinov[§], William A. Goddard III[§] and Ahsanulhaq Qurashi[†, ‡*]

[†] Department of Chemistry, Khalifa University of Science and Technology, Abu Dhabi 127788, UAE

[‡] Center for Catalysis and Separations, Khalifa University of Science and Technology, Abu Dhabi 127788, UAE

[#] Chemical Crystallography Laboratory, Khalifa University of Science and Technology, Abu Dhabi, P.O. Box 127788, UAE

[§] Materials and Process Simulation Center (MSC). California Institute of Technology, Pasadena CA 91125, USA

*Email: ahsan.qurashi@ku.ac.ae,; Tel: +971 2312 4202

*Email: wag@caltech.edu:1-626-833-0036

KEYWORDS. Alloy cluster, nanocluster, gram scale synthesis, crystal structure, atomically precise.

Experimental Section

Materials

Cuprous oxide, tetrafluoroboric acid solution (HBF_4, 48 wt % in water), PETH, PPh_3, p-NP, sodium borohydride ($NaBH_4$), and high performance liquid chromatography (HPLC) grade solvents (acetonitrile, chloroform, methanol, water and hexane) were purchased from Sigma-Aldrich. All chemicals were used directly without further purification.

Synthesis of $[Cu(CH_3CN)_4]BF_4$ complex

Synthesis of $[Cu(CH_3CN)_4]BF_4$ was carried out following a previous publication.[1] 1 g of Cu_2O and 25 mL of CH_3CN was placed in a round bottom flask in the oil bath at 70°C. After 3-5 minutes of stirring, 5 mL of the HBF_4 was added to the solution. The stirring was continued for the next 10-15 min. Later, the hot transparent solution was filtered quickly using a filter paper, and the filtrate was kept in the fridge (0 °C). After 12 h, white crystalline complex, $[Cu(CH_3CN)_4]BF_4$, was collected through filtration followed by two times washing

with diethyl ether. Then the complex was transferred to a sample bottle and stored under vacuum. The complex is highly air sensitive and can change its colour from white to blue under ambient conditions over two months.

Synthesis of Ag_4Cu_{28}

First, 92 mg of $Cu(CH_3CN)_4BF_4$, 12 mg of $AgNO_3$ and 100 mg of PPh_3 were dissolved in a solvent mixture of acetonitrile (4 mL) and chloroform (1 mL). Then, 30 μL of PETH was added. After 5 min, 100 mg of $NaBH_4$ dissolved in 5 mL of methanol was quickly added to the above mixture, and the solution was vigorously stirred for 1 h. The precipitate was collected via centrifugation and redissolved in a solvent mixture of chloroform (4 mL) and hexane (4 mL). This solution was maintained in a glass vial in freeze and dark red crystals (~28 mg) within several days. Yield: ~44% (based on silver).

Gram scale synthesis of Ag_4Cu_{28}

First, 4.6 g of $Cu(CH_3CN)_4BF_4$, 0.6 g of $AgNO_3$ and 5 g of PPh_3 were dissolved in a solvent mixture of acetonitrile (160 mL) and chloroform (40 mL). Next, 1.2 mL of PETH was added. After 5 min, 3 g of $NaBH_4$ dissolved in 220 mL of methanol was quickly added to the above mixture, and the solution was vigorously stirred for 1 h. The precipitate was collected through centrifugation and then redissolved in a solvent mixture of chloroform (100 mL) and hexane (100 mL). This solution was maintained in a freeze and yielded dark red crystals (~1.112 g) within 10 days. Yield: ~35% (based on silver). Formation of Ag_4Cu_{28} NC was confirmed using ESI-MS.

Catalytic hydrogenation of p-nitrophenol (p-NP)

According to the previous literature[2], hydrogenation of p-nitrophenol (p-NP) was chosen as a probe reaction to investigate the catalytic activity of Ag_4Cu_{28}. In a typical experiment, Ag_4Cu_{28} nanocluster (2 mg) was added into the water solution of p-NP (3 ml, 15 mg/L), and the mixture was stirred for 10 min at room temperature. Time-dependent UV-vis absorption spectra were taken after the addition of $NaBH_4$ solid (50 mg, 1.3 mmol). The progress of the reaction was probed by monitoring the change in intensity of p-NP peak at 400 nm as a function of time.

Instrumentation

UV-Vis spectra

UV-Vis spectra were recorded on a Shimadzu UV-2550 spectrophotometer at room temperature. The quartz cuvette of path length 1mm path was used to record the spectra of Ag_4Cu_{28} in DCM.

Electrospray ionization mass spectrometry (ESI-MS)

LC-MS Q Exactive Quadrupole-Orbitrap Mass Spectrometer from the Thermo Fisher Scientific was used for the mass measurement. The Ag_4Cu_{28} NMNCs crystals were dissolved in DCM and the solution was injected directly. The instrument is operated in the mass range of m/z 50–6000 for positive mode and negative mode, respectively. The instrument parameters were maintained as follows: Resolution: 70,000, capillary voltage: 3.0 kV, Aux gas: 10 L/min, Auxiliary gas temperature: 200 °C. The instrument company (Thermo Fisher Scientific) provides built-in software (Xcalibur). This software provides the calculated isotopic patterns.

X-ray photoelectron spectroscopy (XPS)

XPS measurements were performed in a Kratos Axis Ultra DLD spectrometer equipped with a monochromatic Al K_α X-ray source (hν = 1486.6 eV) operating at 150 W, 0.5 mm circular spot size, a flood gun to counter charging effects, and the S3 analysis chamber, a multi-channel plate and delay line detector under a vacuum of ~10^{-9} mbar. All spectra were recorded using an aperture slot of 300 μm x 700 μm. The Survey spectra and high-resolution spectra were acquired by keeping the pass energy of 160 eV and a step size of 1 eV. To avoid differential charging both compounds were arranged in floating mode. Charge neutralization was performed for both samples. Binding energies of C 1s were used as reference and set at 284 eV. The samples were dried properly before creating the vacuum.

Single-crystals X-ray diffraction (SCXRD)

Single crystals of CuAg2507 were crystallized from the mixture of chloroform and n-hexane where n-hexane is used as antisolvent. A suitable crystal was selected and mounted using a Rigaku Oxford Diffraction XtaLAB Synergy-S diffractometer equipped with a HyPix-6000HE Hybrid Photon Counting (HPC) detector and Cu microfocus sealed X-ray tube, as well as a low-temperature Oxford Cryosystems Cobra low temperature device. The crystal was kept at 99.99(11) K during data collection. The data collection strategy was calculated within CrysAlisP (Rigaku OD, 2022; Table S1) to ensure desired data redundancy and percent completeness. Using Olex2[3], the structure was solved with the SHELXT[4] structure solution program using Intrinsic Phasing and refined with the SHELXL[5] refinement package using Least Squares minimization. The space group determination was performed by using PLATON[6]. ORTEP diagrams were generated using ORTEP-3[7]. All non-hydrogen atoms were located in difference-Fourier maps and were then refined anisotropically. All hydrogen atoms were assigned isotropic displacement coefficients U(H) of 1.2U or 1.5U, and their coordinates were allowed to ride on their respective atoms. Least-squares refinement of the structural model was performed under geometric restraints (SADI) and displacement parameter restraints (RIGU, ISOR, SIMU, EADP and DELU) for the surface PET ligands; of these ligands, eight were constrained to idealized hexagons using the AFIX 66 command and one phenyl ring from triphenyl phosphine (TPP) owing to the highly distorted configurations of the phenyl rings. A large space remains between the nanoclusters after assembly, which is occupied by highly disordered solvent molecules (chloroform and/or hexane). These molecules cannot be directly identified from the difference-Fourier map because of the

absence of an assignable model. Therefore, the solvent masking program program implemented in Olex2 was used to remove the electron densities.

Computational details

The density functional theory (DFT) calculations were performed using the Gaussian16 program[8]. Geometry optimization was performed using the B3LYP functional, with the LanL2DZ (Ag and Cu), 6-31G (P, S, and Cl), and 3-21G (C and H) basis sets[9-10]. Tahe VMD program was used for visualization of the optimized structure and isosurfaces of the molecular orbitals[11]. Using the optimized structure, the UV-vis absorption spectrum was calculated via time-dependent DFT (TDDFT) to simulate optical absorption spectra[12].

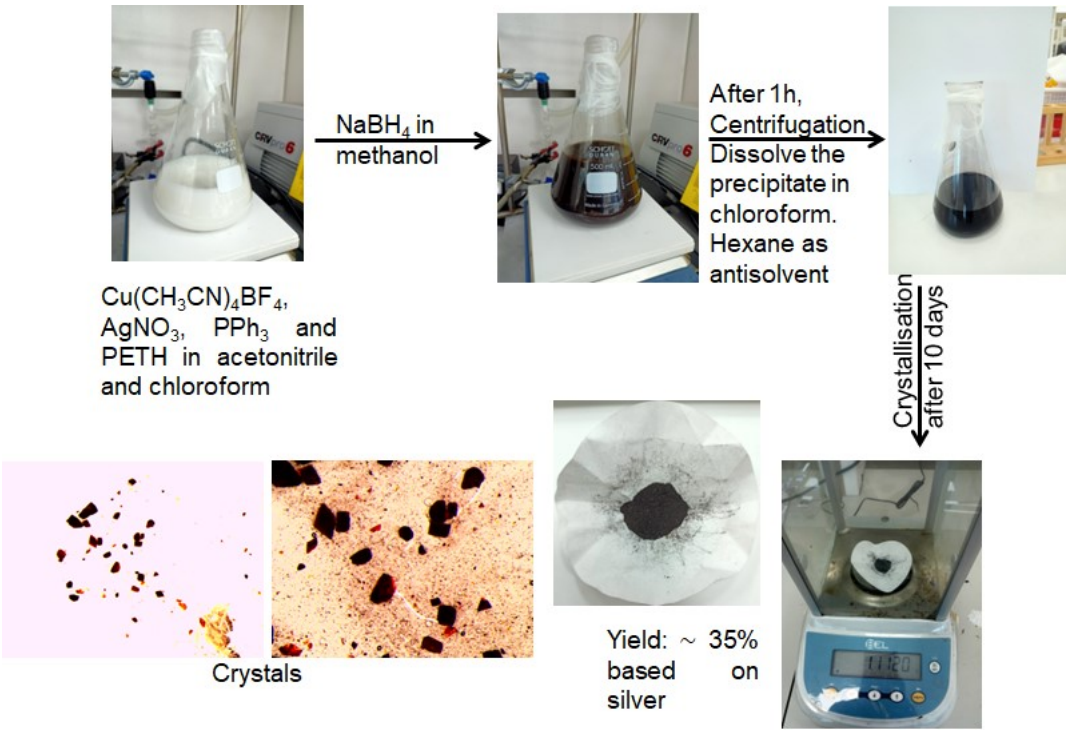

Fig. S1 Gram scale synthesis method of Ag_4Cu_{28} NC.

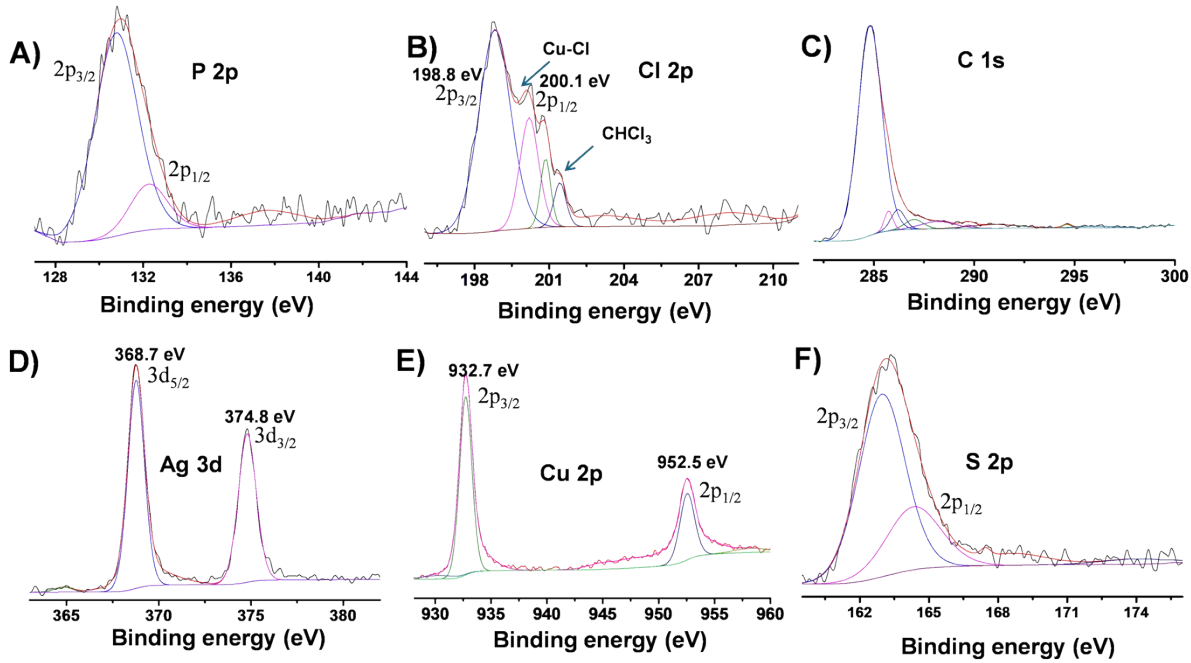

Fig. S2 High-resolution XPS spectra of A) P2p B) Cl2p, C) C1s, D) Ag 3d, E) Cu2p and F) S2p.

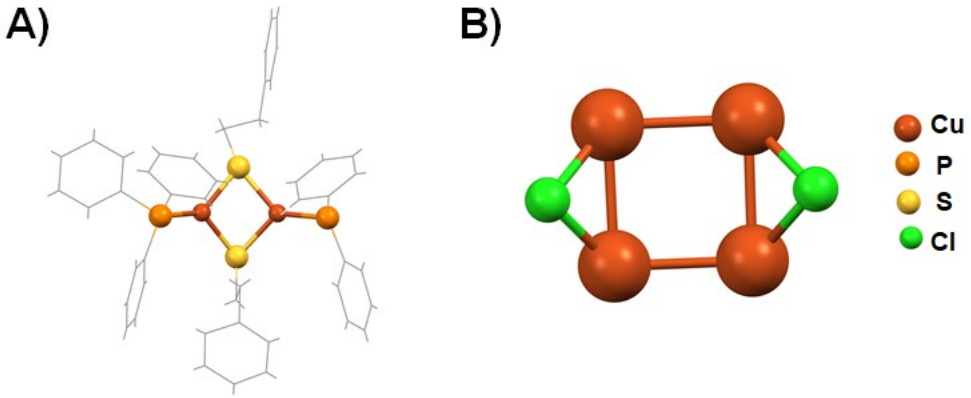

Fig. S3 A) $Cu_2(PET)_2(PPh_3)_2$ motifs and B) Cu_4Cl_2 units.

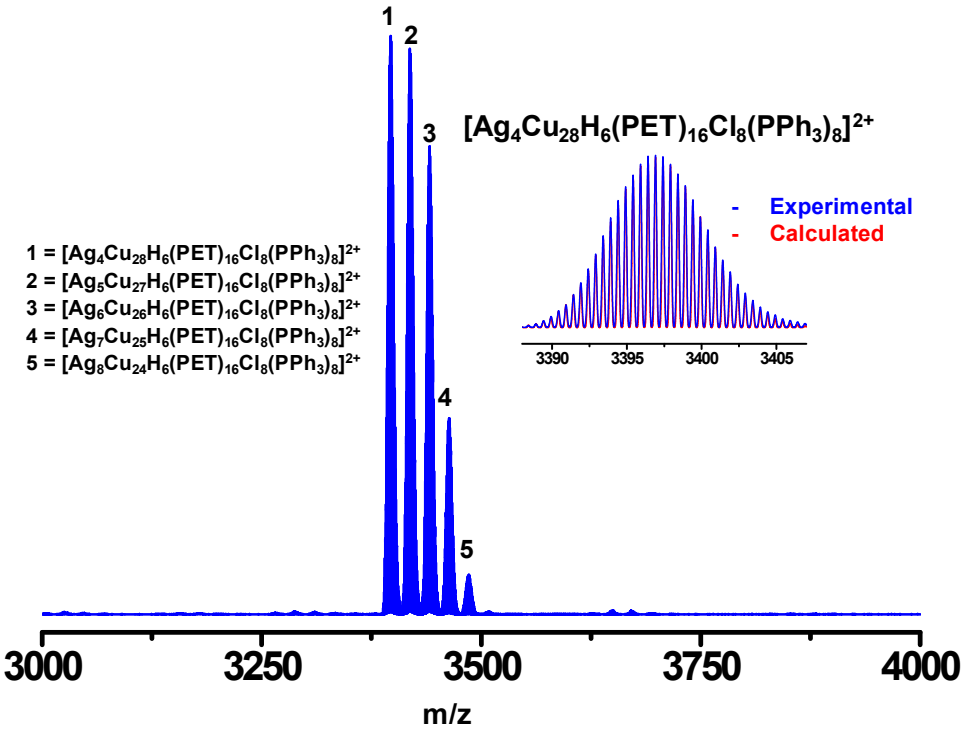

Fig. S4 HR-ESI-MS of Ag_4Cu_{28} NMNC in positive-ion mode after dissolving the crystals in CH_2Cl_2. A comparison of experimental mass spectra of Ag_4Cu_{28} with the simulated is provided in the inset. The observed multiple metal exchange peaks are attributed to a slight positional disorder of Ag and Cu atoms, which also supports the SCXRD data.

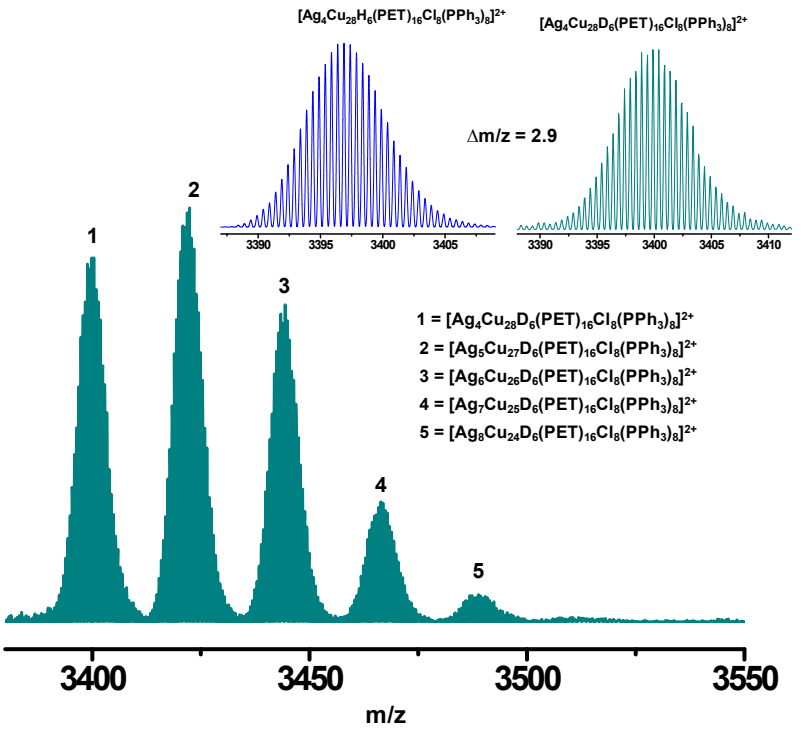

Fig. S5 ESI-MS spectra of $[Ag_4Cu_{28}D_6(PET)_{16}Cl_8(PPh_3)_8]^{2+}$ in positive mode. The mass difference of the isotopic patterns between the $Ag_4Cu_{28}D$ and Ag_4Cu_{28} NC is provided in the inset of Fig. S6.

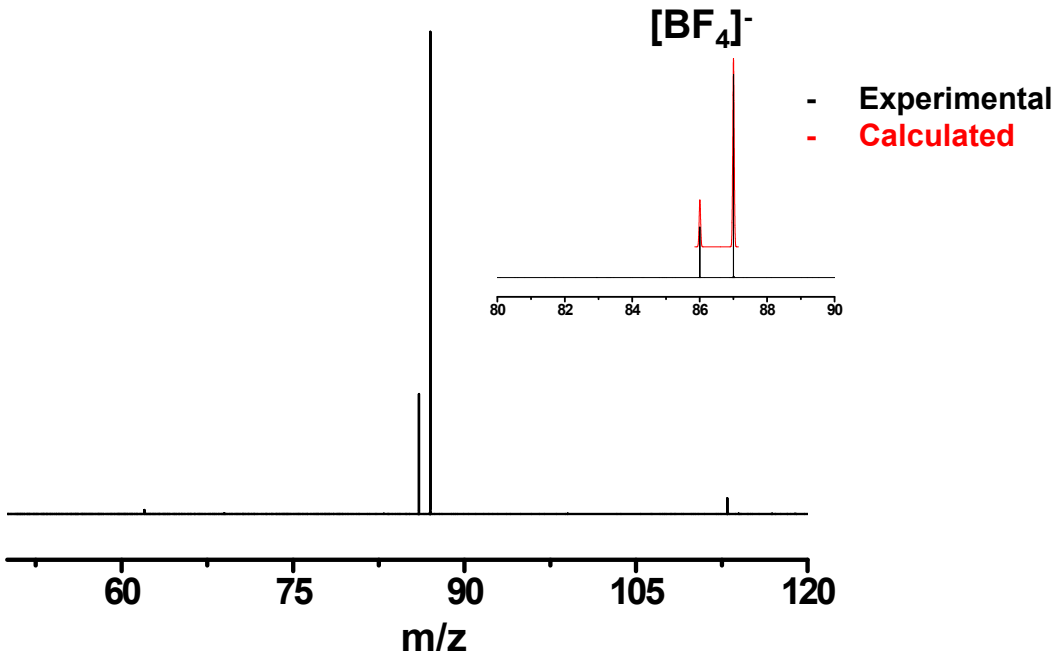

Fig. S6 ESI-MS spectra of BF_4^- in negative mode after dissolving the crystals in DCM. Comparison of experimental mass spectra of BF_4^- with the simulated is provided in the inset of Fig. S7.

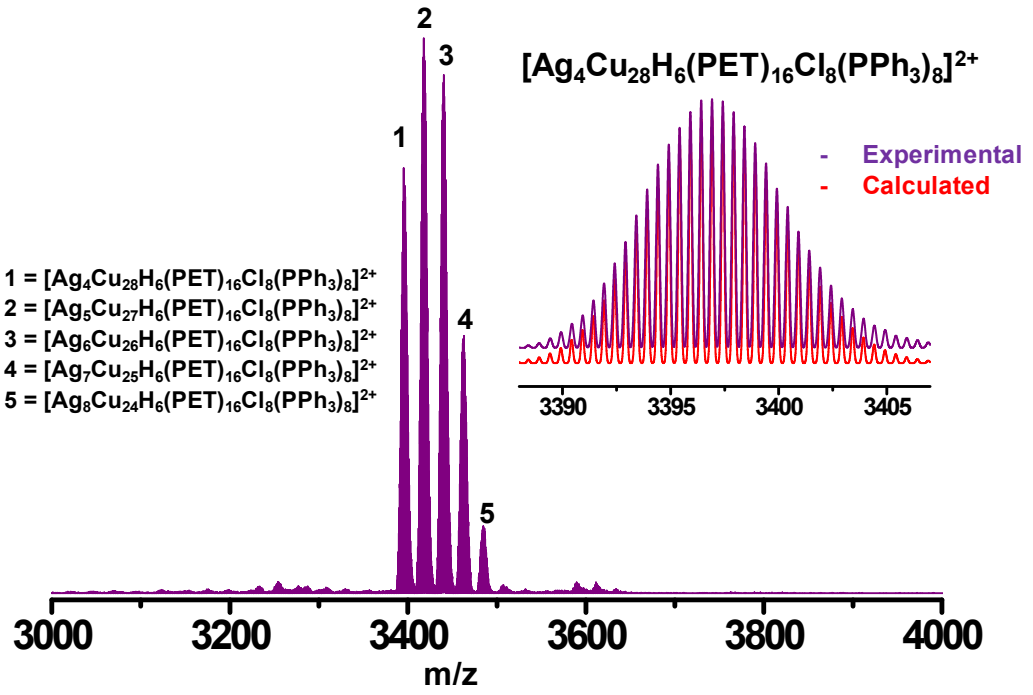

Fig. S7 ESI-MS spectra of Ag_4Cu_{28} NC crystals after sixth month in positive mode after dissolving the crystals in DCM.

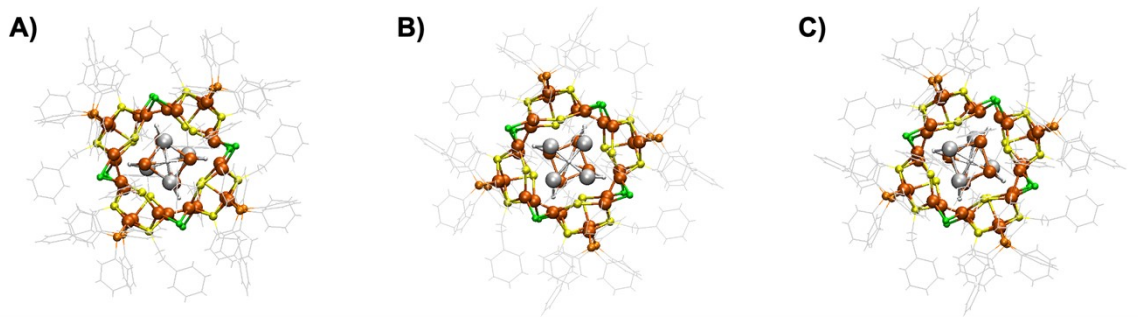

Fig. S8 DFT-optimized structures of Ag_4Cu_{28} with three Ag_4Cu_4 core models, A) Core1, B) Core2, and C) Core3, respectively.

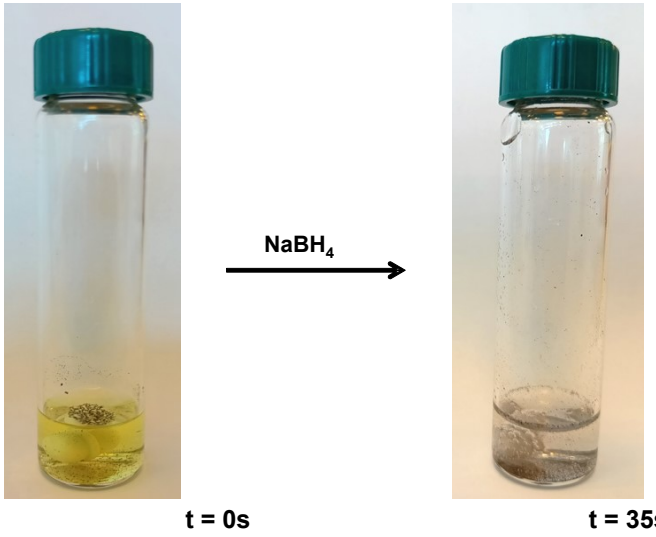

Fig. S9 Photograph of the hydrogenation reaction of p-nitrophenol (pNP) to aminophenol (p-AP) with $NaBH_4$ catalysis within 35s.

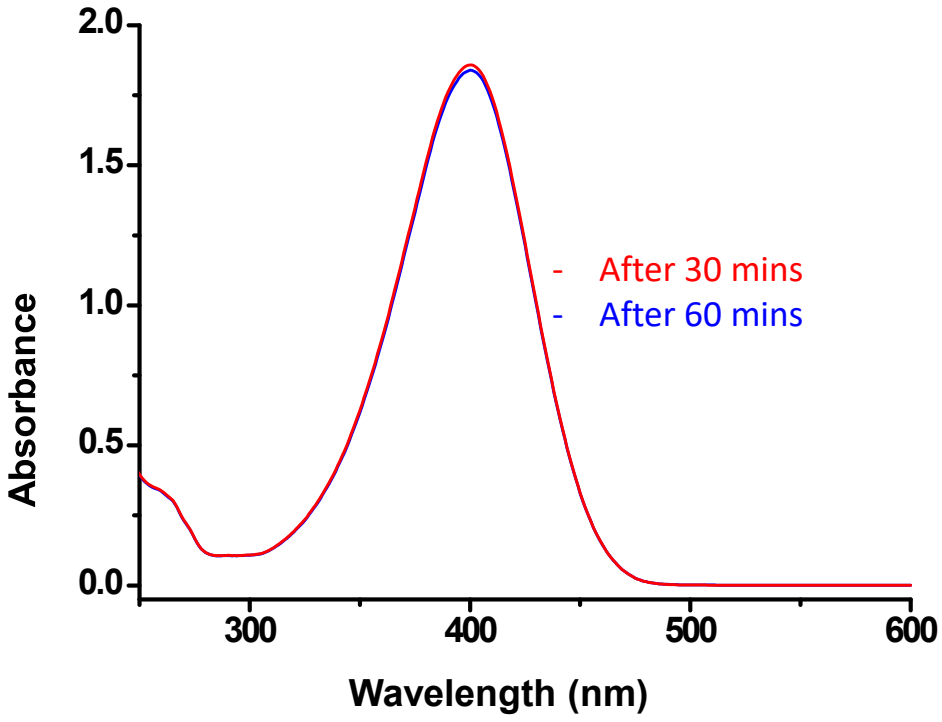

Fig. S10 Time-dependent UV-visible absorption spectra of reduction of p-NP by $NaBH_4$ in the absence of Ag_4Cu_{28} catalyst.

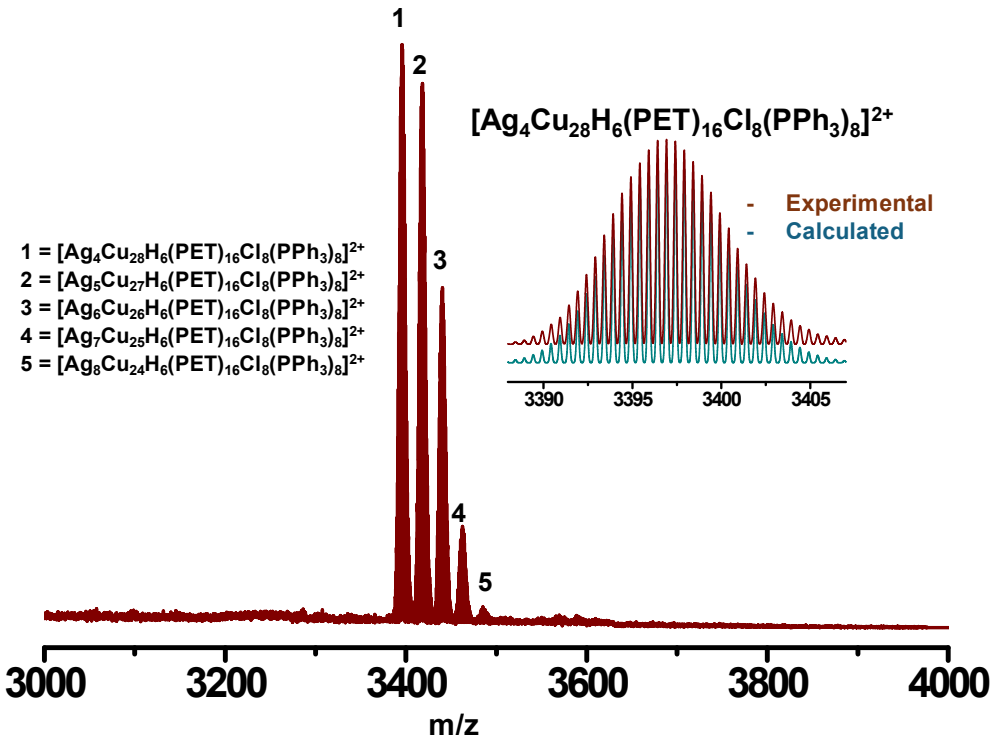

Fig. S11 ESI-MS spectra of $[Ag_4Cu_{28}H_6(PET)_{16}Cl_8(PPh_3)_8]^{2+}$ in positive mode after the catalysis reaction using $NaBD_4$.

Table S1. Crystal and structure refinement data of Ag_4Cu_{28}

Table 1 Crystal data and structure refinement for agcu2507.	
Identification code	agcu2507
CCDC No.	2293022
Empirical formula	$C_{325}H_{377}Ag_4Cl_{32}Cu_{28}P_8S_{16}$
Formula weight	8388.96
Temperature/K	100.15
Crystal system	tetragonal
Space group	*I*4/*m*
a/Å	26.5679(3)
b/Å	26.5679(3)
c/Å	23.7512(5)
α/°	90
β/°	90
γ/°	90
Volume/Å^3	16764.9(5)
Z	2
ρ_{calc}g/cm^3	1.662
μ/mm^{-1}	7.703
F(000)	8494.0
Crystal size/mm^3	0.178 × 0.173 × 0.031
Radiation	CuKα (λ = 1.54184)
2Θ range for data collection/°	4.704 to 150.118
Index ranges	-27 ≤ h ≤ 31, -33 ≤ k ≤ 32, -29 ≤ l ≤ 29
Reflections collected	40133
Independent reflections	8565 [R_{int} = 0.0510, R_{sigma} = 0.0345]
Data/restraints/parameters	8565/1104/708
Goodness-of-fit on F^2	1.095
Final R indexes [I>=2σ (I)]	R_1 = 0.0806, wR_2 = 0.2608
Final R indexes [all data]	R_1 = 0.1003, wR_2 = 0.2920
Largest diff. peak/hole / e Å^{-3}	0.74/-0.63

Table S2. Comparison of catalytic hydrogenation reaction of p-NP to p-AP

Nanocluster used	Rate constant (k) min^{-1}	Reference
$Cu_{11}H_3(Tf\text{-}dpf)_6(OAc)_2$	0.5	13
$[Cu_{57}H_{20}(PET)_{36}(TPP)_4]^+$	0.18	14
$[Cu_{41}(SC_6H_3F_2)_{15}Cl_3(P(PhF)_3)_6(H)_{25}]^{2-}$	6.4	15
$[Ag_4Cu_{28}H_6(PET)_{16}Cl_8(TPP)_8]^{2+}$	7.86	This work

References

1. C. Dong, R.-W. Huang, C. Chen, J. Chen, S. Nematulloev, X. Guo, A. Ghosh, B. Alamer, N. M. Hedhili, T. T. Isimjan, et al., *J. Am. Chem. Soc.* 2021, *143*, 11026-11035.
2. H. Zhou, T. Duan, Z. Lin, T. Yang, H. Deng, S. Jin, Y. Pei, M. Zhu, *Adv. Sci.* **2024**, *11*, 2307085.
3. O. V. Dolomanov, L. J. Bourhis, R. J. Gildea, J. A. K. Howard, H. Puschmann, J. Appl. Crystallogr., 2009, 42, 339-341.
4. G. M. Sheldrick, *Acta Crystallogr. A: Found. Adv.,* 2015, 71, 3-8.
5. G. M. Sheldrick, Acta crystallogr., C Struct. chem., 2015, 71, 3-8.
6. G. M. Sheldrick, Acta crystallogr., C Struct. chem., 2015, 71, 3-8.
7. L. J. Farrugia, Journal of Appled Crystallography 1997, 30, 565–565.
8. M. J. Frisch, G. W. Trucks, H. B. Schlegel, G. E. Scuseria, M. A. Robb, J. R. Cheeseman, G. Scalmani, V. Barone, G. A. Petersson, H. Nakatsuji, X. Li, M. Caricato, A. V. Marenich, J. Bloino, B. G. Janesko, R. Gomperts, B. Mennucci, H. P. Hratchian, J. V. Ortiz, A. F. Izmaylov, J. L. Sonnenberg, D. Williams-Young, F. Ding, F. Lipparini, F. Egidi, J. Goings, B. Peng, A. Petrone, T. Henderson, D. Ranasinghe, V. G. Zakrzewski, J. Gao, N. Rega, G. Zheng, W. Liang, M. Hada, M. Ehara, K. Toyota, R. Fukuda, J. Hasegawa, M. Ishida, T. Nakajima, Y. Honda, O. Kitao, H. Nakai, T. Vreven, K. Throssell, J. A. Montgomery, Jr., J. E. Peralta, F. Ogliaro, M. J. Bearpark, J. J. Heyd, E. N. Brothers, K. N. Kudin, V. N. Staroverov, T. A. Keith, R. Kobayashi, J. Normand, K. Raghavachari, A. P. Rendell, J. C. Burant, S. S. Iyengar, J. Tomasi, M. Cossi, J. M. Millam, M. Klene, C. Adamo, R. Cammi, J. W. Ochterski, R. L. Martin, K. Morokuma, O. Farkas, J. B. Foresman, and D. J. Fox, Gaussian, Inc., Wallingford CT, 2016.
9. A. D. Becke, J. Chem. Phys., 1993, 98, 5648-5652.
10. C. Lee, W. Yang, R.G. Parr, Physical Review B 1988, 37, 785-789.
11. W. Humphrey, A. Dalke, K. Schulten, J. Mol. Graph., 1996, 14, 33–38.
12. C. Adamo, D. Jacquemin, Chem. Soc. Rev., 2013, 42, 845-856.
13. C.-Y. Liu, S.-F. Yuan, S. Wang, Z.-J.Guan, D.-e. Jiang, Q.-M. Wang, *Nat. Commun.* 2022, *13*, 2082.

14. G.-G. Luo, Z.-H. Pan, B.-L. Han, G.-L. Dong, C.-L. Deng, M. Azam, Y.-W. Tao, J. He, C.-F. Sun, D. Sun, *Angew. Chem. Int. Ed.* 2023, *62*, e202306849.
15. H. Zhou, T. Duan, Z. Lin, T. Yang, H. Deng, S. Jin, Y. Pei, M. Zhu, *Adv. Sci.* 2024, *11*, 2307085.